Aalborg Universitet

AALBORG UNIVERSITY
DENMARK

Reduced-Order and Aggregated Modeling of Large-Signal Synchronization Stability for Multi-Converter Systems

Taul, Mads Graungaard; Wang, Xiongfei; Davari, Pooya; Blaabjerg, Frede

Publication date:
2020

Document Version
Accepted author manuscript, peer reviewed version

Link to publication from Aalborg University

Reduced-Order and Aggregated Modeling of Large-Signal Synchronization Stability for Multi-Converter Systems

Mads Graungaard Taul, *Student Member, IEEE,* Xiongfei Wang, *Senior Member, IEEE,*
Pooya Davari, *Senior Member, IEEE,* Frede Blaabjerg, *Fellow, IEEE*

Abstract—During severe grid faults, grid-following converters may become unstable and experience loss of synchronization when complying with requirements for low-voltage ride-through capability. This phenomenon is well-described, understood, and modeled for single-converter systems but lacks a modeling framework when extended to multi-converter systems. To fill this gap, this work presents the necessary stability conditions and aggregated reduced-order models for different multi-converter configurations, which can be used to assess the transient synchronization stability of grid-following converters under symmetrical grid faults. The necessary conditions for transient stability and the aggregated models are verified through numerous simulation studies, which verify their high accuracy for large-signal synchronization stability assessment. To that end, the Anholt wind power plant is considered as a case study where the aggregated model is compared to the full operation of a wind farm string containing 9 full-order grid-following converter models. High model accuracy is obtained, and the computational burden associated with the proposed model is reduced with a factor of 100 compared to a full-order representation on the tested system. Accordingly, the presented analysis and proposed modeling are attractive as a screening tool and a convenient approach for early-stage fault analysis of a system design.

Index Terms—Aggregated Modeling, Grid-Connected Converters, Grid Faults, Reduced-Order Modeling, Synchronization Stability, Transient Stability Analysis.

I. Introduction

WITH the unprecedented integration of renewable energy sources to the modern power system, synchronous generators are being replaced by power-electronics-based generation [1]. With this remarkable transition follow requirements for the responsible operation of power converters and capability to provide ancillary services and low-voltage ride-through (LVRT) support [2]. However, during severe grid faults, the converter control, in particular the synchronization dynamics, may become unstable, even when the LVRT requirements are met [3]. Along these lines, it is outlined by the British network operator, National Grid, that the risk of synchronization instability of phase-locked loop (PLL)-synchronized converters during grid faults is increasing [4]. Consequently, increased

activity in the modeling, analysis, and mitigation of loss of synchronization of converter-based generation is observed [5].

As first outlined in [6], grid-synchronization instability or loss of synchronization (LOS) may occur during weak-grid and severe low-voltage conditions. Under such circumstances, the converter operation acts as a positive feedback loop to its own synchronization process, which in turn makes the PLL unable to remain synchronized with the external grid voltage [7]. Since this issue happens during large disturbances, small-signal linearized models cannot be adopted to represent the transient instability problem. For that reason, much work has been devoted to model and analyze LOS using the nonlinear dynamics governing the synchronization process. A necessary condition for transient stability was derived in [6], which highlights the root-cause of large-signal synchronization instability. This model is based on steady-state conditions which cannot be used for transient stability analysis when the necessary condition is met. To address this, the authors in [7] proposed a quasi-static large-signal model of a PLL-synchronized converter under grid faults. Building on the foundation of this quasi-static large-signal model, numerous work has been done to describe and model LOS [8]–[12] alongside motivating ideas for LOS mitigation strategies [3], [13]–[18]. Also, since the nonlinear model has no known analytical solution, nonlinear graphical tools and numerical approximations have been used to assess the transient stability [19]–[22].

Nonetheless, all of the cited publications for modeling of PLL-synchronized grid-following converters under large-signal disturbances are based on a single-converter-infinite-bus representation. Therefore, the developed models can only be used to represent one single system and cannot capture the behavior of paralleled or more complicated multi-converter systems. Regarding modeling of multi-converter systems with focus on the synchronization dynamics, some previous work has been performed [23]–[28] where [23]–[26] focus on the small-signal behavior. A large-signal model is presented in [27], but here all converters are assumed to share the same point-of-synchronization (POS) and point-of-connection (POC), which significantly reduces its usage for practical applications. Lastly, the authors in [28] present a large-signal model for paralleled converters without any assumptions on a shared POS or POC. However, the model in [28] is only defined for two paralleled units, where a generalization for n converters seems too cumbersome since

the frequency dynamics of all converters are coupled with each other. Capturing these couplings for multiple converters and complex interconnections become impractical and time-consuming. Therefore, in regards to the modeling of large-signal synchronization stability of grid-following multi-converter systems, a generalized modeling framework is still lacking from the existing literature. To that end, an aggregated method that can accurately capture the collective synchronization dynamics of multi-converter systems without considering the couplings between all interconnected units is needed.

A. Model Aggregation

In regards to aggregated modeling of multi-converter systems and wind farms, this is not a new area of study [29]. For analysis of the internal stability of multi-converter systems, detailed models are considered [30], whereas aggregated models are often used to investigate the impact that a wind farm or large-scale system has on the connected power system [31]. The aggregation procedure usually involves developing an aggregated representation of the converters (either single-machine or multi-machine representation), an equivalent impedance preserving the power flow of the system, and an equivalent representation of the stochastic energy yield [32], [33]. For aggregation, single-turbine aggregation is often considered insufficient in terms of accuracy, which is why multi-machine aggregation is usually performed for transient studies [34]. For the multi-machine aggregation, many methods focus on how to perform proper clustering of converters [35]. This includes K-means clustering [36], support vector clustering [37], multi-objective optimization algorithm [35], simple clustering based on similar wind speeds [38], or clustering through coherency equivalence [39], [40]. Thus, much research focuses on the clustering based on the incoming wind speed used for small-signal analysis rather than simplified assessment of converter synchronization stability during severe grid faults.

To that end, most presented aggregated models employ the full-order dynamics of the aggregated converters [41], resulting in more complexity compared to reduced-order aggregated models. In [42], a reduced-order aggregated structure is presented to characterize the small-signal frequency support of aggregated wind turbines. Also, an aggregation model for a DFIG-based wind farm is proposed in [43] to study the low-frequency power oscillations. However, these dynamic models are based on transfer functions and only the small-signal angular stability is assessed.

B. Research Gaps and Contributions

Despite a lot of research on aggregated modeling, the above works are not explicitly focused on the synchronization stability during grid faults, for which further simplifying assumptions can be made to effectively reduce the computational burden. During severe fault conditions, all converters can provide 1 pu of reactive current support, despite their initial wind speed. Hence, when studying severe faults, a highly simplified reduced-order aggregated model can be developed to assess the large-signal synchronization stability, as is pursued in this work. Up until now, the aggregated models are developed to replicate the dynamics of the PCC [29]. On the contrary, this paper aims to present an aggregated model to describe the internal synchronization stability of the multi-converter system in an aggregated reduced-order manner, such that fast transient instability screening can be performed and a physical understanding of the instability phenomenon can be obtained.

Besides representing the converter as an ideal current source, oriented by the PLL dynamics, this work also shows that the outer dc-link voltage control and AC voltage control can be neglected from the model when focusing on the synchronization stability under grid faults. This is different from other reduced-order modeling approaches such as singular perturbation theory, used to neglect the fast dynamics of the model [44]. In such work, using the converter operation under the fault behavior to reduce the outer power loops cannot be performed since they belong to slow preserved modes.

Therefore, even though much research has been done on aggregation and reduced-order modeling of multi-converter systems, the modeling has not been focused on severe grid faults. In this case, the modeling may accurately use the fault conditions to employ assumptions, leading to a highly simplified structure, which still preserves the collective internal synchronization dynamics of the system. This is the motivation and approach pursued in this work. Finally, in addition to this, disclosing how the paralleled converter operation changes the physical interpretation and necessary stability conditions of the system has so far not been described.

Thus, this paper aims to fill these research gaps by considering three system configurations that cover most multi-converter configurations. For these configurations, the necessary conditions for transient stability are derived. These conditions are beneficial for two reasons. First, the necessary conditions serve as a reliable tool to understand and assess the transient stability and, secondly, the q-axes voltage components, used to derive the necessary conditions, lay the foundation for developing reduced-order dynamic models for each configuration. In contrary to previous work on LOS, the influence of network capacitance on the necessary stability condition is also revealed. To avoid modeling the coupling dynamics between all interconnected units and the time-complexity of doing so, this work presents an aggregated reduced-order large-signal model for a daisy-chain configured system, e.g., as used in large offshore wind farms, for transient stability assessment.

Accordingly, the research contributions can be summarized as:

1) Identification of necessary stability conditions for the three descriptive paralleled converter system configurations.
2) Extension of these conditions to reduced-order large-signal scalable models, which are designed for a low-order transient stability assessment tool.
3) For daisy-chain collector systems where converters are separated by non-negligible impedances, an aggregated reduced-order large-signal model is proposed. This model eliminates the need to model all couplings between the interconnected units, brings a high model accuracy, and therefore reduces the computational re-

quirements by a factor of 100 when compared to a detailed simulation study on a real functioning wind farm.

4) Showing that the outer power loops of the converters can be neglected for the stability assessment under severe grid faults and that the presented method also provides accurate assessments under heterogeneous converter operation.

The remainder of this paper is structured as follows: Section II presents the necessary conditions for transient stability of three representative multi-converter configurations. Also, how potential network shunt capacitances influence the static stability limits is analyzed. In Section III, the q-axes voltage components used to derive the necessary stability conditions are merged with the dynamics of the PLL to establish large-signal reduced-order models for all system configurations. Additionally, a proposed aggregated model for analyzing the transient stability for e.g., a wind farm collector system is presented. All necessary conditions and large-signal models are numerically verified in Section IV, whereas a case study on the Anholt offshore wind farm is conducted in Section V to verify the proposed aggregated model further. Here, the proposed reduced-order aggregated model is also verified under heterogeneous converter operation. Finally, concluding remarks are enclosed in Section VI.

II. STATIC STABILITY LIMITS

The static limitation or necessary condition for transient stability is evaluated for three representative configurations of paralleled converters: converters with a common point of synchronization (POS) and point of connection (POC), converters with a different POS but common POC, and converters with different POS and POC. These together form a representative platform for literally any multi-converter system. Hence, from a system configuration point of view, the models presented in this work will be general and scalable. The static models reveal the fundamental instability phenomenon and are, therefore, relevant when assessing the large-signal synchronization stability. To that end, the formulations used to develop the necessary stability conditions are also the fundamental building blocks for constructing the reduced-order large-signal models. The assumptions made for the derivation of the static and dynamic models presented in this work are the following:

1) All converters have homogeneous dynamics, i.e., the converter topology, the control law, the controller parameters, and the output current are all the same.
2) Outer power loops are not included and can be neglected during severe faults.
3) The converter operation is represented as an ideal controllable current source, which is oriented using the PLL dynamics.

The first assumption implies that the presented models only applies to multi-converter systems where the converters possess a high degree of similarity. Since paralleled converters used in renewable applications such as wind and solar might be exposed to different wind speeds and solar irradiance, the injected currents from the paralleled converters might not
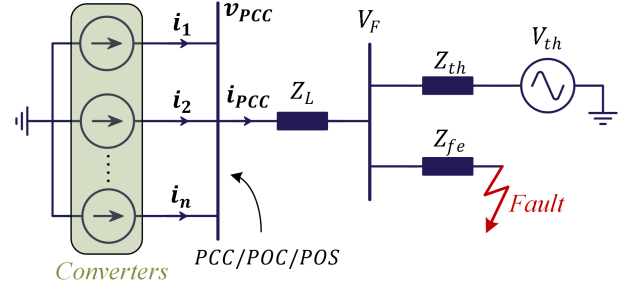

Fig. 1. Simplified single-line diagram of paralleled converters injecting current into an external grid. Here, the parallel converters have a common point of synchronization (POS) and point of connection (POC), here at the PCC.

be equal. However, during severe faults, where the network voltages drop low and a breaking chopper takes care of the active power from the renewable energy source, all converters can supply rated reactive current, which justifies the assumption of equal currents during the fault. To that end, during severe faults, where the POS voltage is low, converters should prioritize 1 pu of reactive current injection to support the local network voltage [2]. Considering this, then assumption 2 can be justified. Lastly, assumption 3 can be justified for two reasons. First, the dominating dynamics of loss of synchronization lies in the low-frequency range [22], [45]. Secondly, the bandwidth of the inner current regulator is usually placed much higher than that of the synchronization process, which facilitates that they can be analyzed individually [7], [14], [15]. To that end, only symmetrical faults are considered for this study. This is done since during a worst-case asymmetrical fault (a double line-to-ground fault [46]), the resulting positive and negative sequence voltage magnitudes at the fault location never drop below $1/3$ pu, which implies that the converters is unlikely to operate at an unstable operating point during the fault. Thus, unbalanced faults do not pose any threat for the instability mechanisms studied in this paper

A. Parallel Converters with Common Point of Synchronization and POC

The simplest configuration of the paralleled operation is shown in Fig. 1 where n paralleled converters inject current into an external grid. The external grid consists of a line impedance Z_L and an equivalent Thevenin grid (Z_{th}, V_{th}) with a parallel feeder branch where a symmetrical fault is considered to occur. Z_{fe} denotes the combined feeder and fault impedance. Such a parallel configuration with a shared POS could represent paralleled photovoltaic (PV) inverters and other paralleled systems that are located in an electrical vicinity of each other. The voltage at the PCC can from the superposition of the linear network be expressed as

$$\boldsymbol{v_{PCC}} = K_g(\omega_g)V_{th}e^{j(\theta_g+\phi_g)} + K_c(\omega_1)I_1e^{j(\theta_{C1}+\phi_{c1})}$$
$$+ K_c(\omega_2)I_2e^{j(\theta_{C2}+\phi_{c2})} + \cdots + K_c(\omega_n)I_ne^{j(\theta_{Cn}+\phi_{cn})} \quad (1)$$

which succinctly can be written as

$$\boldsymbol{v_{PCC}} = K_g(\omega_g)V_{th}e^{j(\theta_g+\phi_g)} + \sum_{i=1}^{n} K_c(\omega_i)I_i e^{j(\theta_{Ci}+\phi_{ci})}, \tag{2}$$

with [5]

$$K_g(\omega_g) = \left| \frac{\boldsymbol{Z_{fe}}(\omega_g)}{\boldsymbol{Z_{fe}}(\omega_g) + \boldsymbol{Z_{th}}(\omega_g)} \right|, \tag{3}$$

$$K_c(\omega_i) = \left| \boldsymbol{Z_L}(\omega_i) + \frac{\boldsymbol{Z_{fe}}(\omega_i)\boldsymbol{Z_{th}}(\omega_i)}{\boldsymbol{Z_{fe}}(\omega_i) + \boldsymbol{Z_{th}}(\omega_i)} \right|, \tag{4}$$

$$\phi_g(\omega_g) = \angle\left(\frac{\boldsymbol{Z_{fe}}(\omega_g)}{\boldsymbol{Z_{fe}}(\omega_g) + \boldsymbol{Z_{th}}(\omega_g)} \right), \tag{5}$$

$$\phi_c(\omega_i) = \angle\left(\boldsymbol{Z_L}(\omega_i) + \frac{\boldsymbol{Z_{fe}}(\omega_i)\boldsymbol{Z_{th}}(\omega_i)}{\boldsymbol{Z_{fe}}(\omega_i) + \boldsymbol{Z_{th}}(\omega_i)} \right), \tag{6}$$

where ω_i is the estimated frequency by the ith converter, θ_g is the angle of V_{th}, $\theta_{Ci} = \theta_{PLLi} + \theta_I$ is the angle of the injected current vector of the ith converter, and θ_I is the power factor angle. During severe faults, the converters should inject 1 pu of reactive current to support the local voltages [2]. Hence, θ_I can be assumed to be equal for all converters. It should be noted that since the paralleled converters in Fig. 1 all share the same PCC where the synchronization is performed; they can be assumed to have the same estimated angle from the PLL which in steady-state satisfies that $\theta_{PLL} = \theta_{PCC}$. This also implies that $\theta_{C1} = \theta_{C2} = \cdots = \theta_{Cn}$, provided that the currents of the paralleled converters are the same. From this, the PCC voltage can be expressed in the shared rotating frame (multiplying with $e^{-j\theta_{PLL}}$ on both sides of (1)). This will cancel θ_{PLLi} from θ_{Ci}. Then, by evaluating the imaginary part, the q-axis component of $\boldsymbol{v_{PCC}}$ can be obtained as

$$v_{PCC,q} = \underbrace{K_g(\omega_g)V_{th}\sin(\theta_g + \phi_g(\omega_g) - \theta_{PLL})}_{\text{Grid-Synchronization Term, } v_{q-}}$$
$$+ \underbrace{nK_c(\omega_{PLL})I_C\sin(\theta_I + \phi_c(\omega_{PLL}))}_{\text{Self- and Cross-Synchronization Terms, } v_{q+}}, \tag{7}$$

where I_C is the magnitude of the current vector injected by each of the n converters. From (7), it can be seen that each converter when measuring the PCC voltage sees the contribution from the equivalent grid and the contribution from all the other converters, i.e., an increased self- and cross-synchronization term. This implies that seen from each converter, the equivalent grid impedance seems n times larger compared to the case where only one converter is considered. This is consistent with the findings of the linearized systems in [27], [47], [48]. This is intuitive as each current contribution from all of the paralleled units generates a voltage drop in the line impedance Z_L. Accordingly, the synchronization process of each converter becomes harder than that of a single-converter system, since the PCC voltage is not only dependent on the external grid voltage, but also the voltage drops on Z_L generated by the $n-1$ neighboring converters.

For a stable operating point to exist, a solution for θ_{PLL}, which assures that $v_{PCC,q} = 0$ must exist. Using this, one can derive a necessary condition for the large-signal synchro-
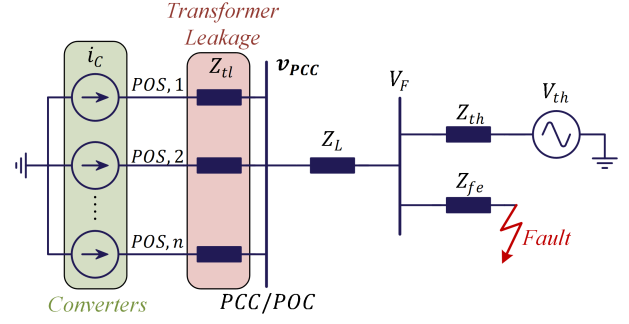

Fig. 2. Simplified single-line diagram of paralleled converters with different points of synchronization but a common point of connection (POC), i.e., PCC.

nization stability. This is the static stability condition for the maximum current magnitude that can be injected as

$$I_C \leq \frac{V_{th}K_g(\omega_g)}{nK_c(\omega_{PLL})|\sin(\theta_I + \phi_c(\omega_{PLL}))|}. \tag{8}$$

From (8), it can be seen that the issues encountered for weak-grid conditions for a single-converter system are exacerbated when multiple parallel converters are considered.

B. Parallel Converters with Different Point of Synchronization but Common POC

For the second configuration where the parallel converters experience different POS, i.e. the place where the voltage measurement is fed to the PLL, but share a common POC is shown in Fig. 2. Here, the POS is located on the low-voltage side of e.g. the wind turbine step-up transformer. Consequently, the voltage measurement provided to the synchronization unit will be different from the previous case as the injected currents of each converter have a stronger coupling to the voltage at the POS and globally a weaker coupling to the external grid. The POS voltage of the n paralleled converter in Fig. 2 can be expressed as

$$\boldsymbol{v_{POS,1}} = \boldsymbol{v_{PCC}} + I_1 Z_{tl,1} e^{j(\theta_{C1}+\phi_{tl,1})},$$
$$\vdots$$
$$\boldsymbol{v_{POS,n}} = \boldsymbol{v_{PCC}} + I_n Z_{tl,n} e^{j(\theta_{Cn}+\phi_{tl,n})}. \tag{9}$$

Inserting the expression for the PCC voltage from (2), the POS voltage at the pth converter becomes

$$\boldsymbol{v_{POS,p}} = K_g(\omega_g)V_{th}e^{j(\theta_g+\phi_g)} + \sum_{i=1}^{n} K_c(\omega_i)I_i e^{j(\theta_{Ci}+\phi_{ci})}$$
$$+ I_p Z_{tl,p} e^{j(\theta_{Cp}+\phi_{tl,p})}. \tag{10}$$

Assuming equal leakage inductances of all the step-up transformers, the q-axis component of each POS voltage becomes

$$v_{POS,q} = \underbrace{K_g(\omega_g)V_{th}\sin(\theta_g + \phi_g - \theta_{PLL})}_{\text{Grid-Synchronization Term, } v_{q-}}$$
$$+ \underbrace{I_C n K_c(\omega_{PLL})\sin(\theta_I + \phi_c(\omega_{PLL}))}_{\text{Self- and Cross-Synchronization Term, } v_{q+1}}$$
$$+ \underbrace{I_C Z_{tl}(\omega_{PLL})\sin(\theta_I + \phi_{tl}(\omega_{PLL}))}_{\text{Additional Self-Synchronization Term, } v_{q+2}} \tag{11}$$

From (11), it can be noticed that the positive feedback term or self- and cross-synchronization term is further increased compared to (7) due to the included step-up transformer. Accordingly, the limit for the injected currents then becomes constrained to

$$I_C \leq \frac{V_{th}K_g(\omega_g)}{|nK_c(\omega_{PLL})\sin(\theta_I + \phi_c(\omega_{PLL})) + X_{tl}(\omega_{PLL})\cos(\theta_I)|}, \tag{12}$$

neglecting transformer resistance. During purely reactive current injection ($\theta_I = -90°$) as specified by grid codes during severe grid faults, the static stability constraint in (12) is identical to (8). This is because the resistance of the transformer is neglected and the dynamic behavior of the current controller is assumed ideal for this static model. For actual implementation, the system with the transformer will be more prone to instability as the dynamics of the system become slower, meaning that the assumption of an ideal controllable current source for the converter becomes less valid. Also, during a severe fault event, the converter has to change its injected currents from active to capacitive reactive. This transition involves some transient behavior where the second term in the denominator in (12) will be non-zero, which increases the value of the denominator in the transient part. The worst-case is at the fault instant where $\cos(\theta_I) = 1$, whereas $\cos(\theta_I) \to 0$ as the current controller settles, usually in a few milliseconds.

C. Parallel Converters with Different Point of Synchronization and POC

Parallel converters may topologically be interfaced such that they neither share the same POS nor the same POC. An example of this is a wind farm string or collector system as shown in Fig. 3, where each converter is connected in parallel along a string separated by collector impedances, denoted Z_c. This is also known as a daisy-chain turbine configuration. As depicted in Fig. 3, each of the m paralleled wind farm strings consists of n internal converters. It should be mentioned that for offshore wind farm applications, the PCC point is often referred to as the point of the right-hand side of the transport line/cable Z_L in Fig. 3. However, to be consistent with the previous diagrams, the PCC point is continued to be referred to as the point in the wind farm where all the parallel collector grids are connected. The POS voltage at the pth wind turbine can be expressed as

$$\boldsymbol{v_{POS,p}} = \boldsymbol{v_{PCC}} + \sum_{i=1}^{p}\left(Z_{c,i}e^{j\phi_{col,i}}\sum_{j=i}^{n}I_je^{j\theta_{Cj}}\right) + I_pZ_{tl,p}e^{j(\theta_{Cp}+\phi_{tl,p})}, \tag{13}$$

where ϕ_{col} is the impedance angle of the collector cable, n is the number of turbines on the string, and $n \geq p \geq 1$ is the POS number of the wind turbine voltage counting from the PCC towards the end of the string. During a severe grid fault, all converters in the wind farm string can supply 1 pu of reactive current. This is true even though each converter at the pre-fault operating point may have significantly different injections of active current based on different wind speeds and wake effects in the wind farm. To that end, as the collector
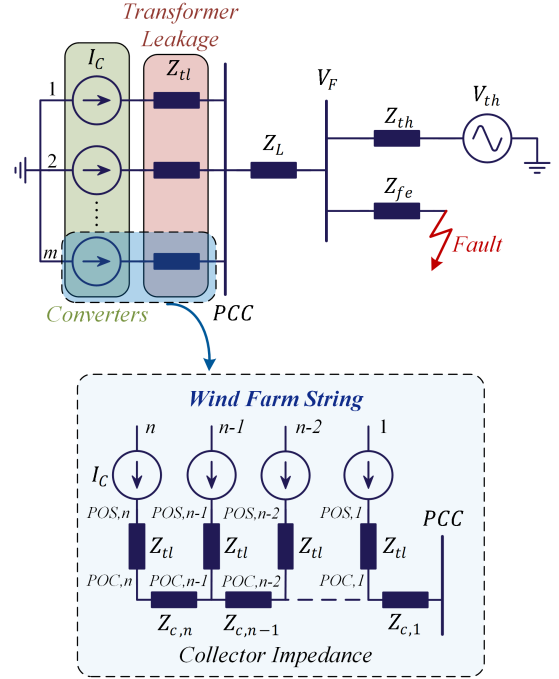

Fig. 3. Simplified single-line diagram of paralleled converters in wind farm radial string with different points of synchronization (POS) and point of connections (POC). Each converter is interconnected through collector impedances represented as $Z_{c,i}$

impedances usually are much smaller compared to the wind farm park transformer, the phase-angle difference between the injected currents from the n converters is also small. Thus, it can be assumed that the injected currents from the paralleled converters have the same magnitude and phase (I_C and θ_I). Based on the assumption of small-angle differences along the string and that each converter in steady-state is synchronized to its POS voltage, the PLL phase-angles are equal as $\theta_{PLL1} = \theta_{PLL2} = \cdots = \theta_{PLLn} = \theta_{PLL}$. Using the assumptions described above and multiplying each side with $e^{-j\theta_{PLL}}$, θ_{Ci} reduces to θ_I. Using the expression for the PCC voltage in (2) and taking the imaginary part of the POS voltage at the pth wind turbine, one can get that

$$\begin{aligned} v_{POS,q,p} = {} & K_gV_{th}\sin(\theta_g + \phi_g - \theta_{PLL}) \\ & + mK_cI_s\sin(\theta_I + \phi_c) + I_CZ_{tl}\sin(\theta_I + \phi_{tl}) \\ & + \sum_{i=1}^{p}Z_{c,i}I_C(n-i+1)\sin(\theta_I + \phi_{col,i}) \end{aligned} \tag{14}$$

where m is the number of parallel strings, I_s is the total string current magnitude of the m paralleled strings, and Z_{tl} is considered equal for all converters. To develop a single necessary condition for the whole string, the location in the wind farm string, which is most susceptible to loss of synchronization is considered. The worst-case location along the wind farm string will be at the end, i.e., at the nth converter. This is true since this will create the largest positive feedback in the PLL synchronization loop as it is evident from (14). Then, if the nth converter can be guaranteed to operate at a stable equilibrium point, so can the remaining units in the

string too. Accordingly for the nth converter, the POS voltage is

$$v_{POS,q,n} = \underbrace{K_g V_{th} \sin(\theta_g + \phi_g - \theta_{PLL})}_{\text{Grid-Synchronization Term, } v_{q-}}$$
$$+ \underbrace{m K_c I_s \sin(\theta_I + \phi_c)}_{\text{Mutual-String Interaction Term, } v_{q+1}} + \underbrace{I_C Z_{tl} \sin(\theta_I + \phi_{tl})}_{\text{Transformer Leakage Term, } v_{q+2}}$$
$$+ \underbrace{\sum_{i=1}^{n} Z_{c,i} I_C (n - i + 1) \sin(\theta_I + \phi_{col,i})}_{\text{Self-String Interaction Term, } v_{q+3}}. \quad (15)$$

For the q-axis voltage component to be zero, the first term on the right-hand side must be sufficient to cancel the remaining offsetting terms. From this, and assuming that $I_s = n I_C$, the necessary stability condition becomes

$$I_C \leq \frac{V_{th} K_g}{|A|}, \quad (16)$$

where

$$A = nm K_c \sin(\theta_I + \phi_c) + Z_{tl} \sin(\theta_I + \phi_{tl})$$
$$+ \sum_{i=1}^{n} (n - i + 1) Z_{c,i} \sin(\theta_I + \phi_{col,i}), \quad (17)$$

and K_g, K_c, ϕ_c, Z_{tl}, ϕ_{tl}, Z_c, and ϕ_{col} are frequency-dependent variables. For the case where the collector grid impedances are identical, A reduces to

$$A = nm K_c \sin(\theta_I + \phi_c) + Z_{tl} \sin(\theta_I + \phi_{tl})$$
$$+ \frac{Z_c(n + n^2)}{2} \sin(\theta_I + \phi_{col}). \quad (18)$$

As can be noted from the first term in (17) and (18), each paralleled string is considered to consist of n converters. This is a strong assumption, which may not be applicable in practice since different strings may have a different number of converters. However, the factor nm in the above terms can simply be replaced with n_{tot}, representing the total number of converters in the paralleled strings.

D. Influence of Cable Capacitance

For offshore wind farms and due to the public opposition to overhead lines on land, submarine and land cables are often used for the connection and interconnection of wind turbines and wind farms. This implies that the cable capacitance may not be neglected since it can be 20-50 times higher than for the capacitance for overhead lines [49]. Therefore, the impact that this non-negligible capacitance has on the static stability limit must be evaluated. Considering one single converter from Fig. 1 where the line impedance (Z_L) is approximated with a cable $\Pi-$model, the static limitation for current transfer can be written as

$$I_{PCC} \leq \frac{V_{th} K_{gc}(\omega_g)}{K_{cc}(\omega_{PLL}) |\sin(\theta_I + \phi_{cc}(\omega_{PLL}))|}, \quad (19)$$

where

$$K_{gc} = \left| \frac{Z_C{}^2 Z_{fec}}{K_1} \right|, \quad \phi_g = \angle \left(\frac{Z_C{}^2 Z_{fec}}{K_1} \right), \quad (20)$$

$$K_{cc} = \left| \frac{Z_C(Z_L Z_{fe} Z_{th} + Z_C(Z_L Z_{th} + Z_{fe}(Z_L + Z_{th})))}{K_1} \right|, \quad (21)$$

$$\phi_{cc} = \angle \left(\frac{Z_C(Z_L Z_{fe} Z_{th} + Z_C(Z_L Z_{th} + Z_{fe}(Z_L + Z_{th})))}{K_1} \right), \quad (22)$$

and

$$K_1 = Z_C{}^2(Z_{fe} + Z_{th}) + Z_C(Z_L Z_{th} + Z_{fe}(Z_L + 2Z_{th}))$$
$$+ Z_L Z_{fe} Z_{th}, \quad (23)$$

and $Z_C = 1/(0.5 j \omega C)$ since half of the capacitance is distributed at each end of the line. During pure reactive current injection ($\theta_I = -90°$), the static stability margin is determined by the ratio between $V_{th} K_{gc}$ and $\Re\{K_{cc}\}$. For analytical simplicity, it is assumed that the converter operation does not influence the voltage at the fault location ($Z_{fe} \approx 0$), then

$$\Re\{K_{cc}\} = \frac{R_L}{1 + (0.5C\omega)^2(R_L^2 + L_L^2(\omega^2 - \omega_{LC}^2))}, \quad (24)$$

where $\omega_{LC} = 1/\sqrt{L_L C}$. Since the LC resonance frequency is indeed much higher than the network operating frequency, (24) can be approximated as

$$\Re\{K_{cc}\} = \frac{R_L}{1 + (0.5C\omega)^2(R_L^2 - (L_L \omega_{LC})^2)}. \quad (25)$$

Hence if $R_L > L_L \omega_{LC}$, then the real part will be reduced from R_L, which increases the stability margin, whereas if $R_L < L_L \omega_{LC}$, the real part of K_{cc} will be increased, which reduces the stability margin. However, it should be noted that this term is multiplied with $(0.5C\omega)^2$, which in practice is a very small number. As an example, using the cable data in [50] for the type 2XS(FL)2YRAA 18/30(36) kV, one will find that for the smallest and largest conductor sizes, the change in $\Re\{K_{cc}\}$ from R_L only exceeds 5% when the cable length is increased above 35-50 km. Hence, for this study involving interconnecting cables between wind turbines in wind farms, which are much shorter, the use of the static stability limits without considering the effect of the cable capacitance is well justified.

III. AGGREGATED REDUCED-ORDER LARGE-SIGNAL MODELS OF SYSTEM CONFIGURATIONS

The static stability limits derived for the different system configurations represent the necessary condition for large-signal synchronization stability. Besides these models being useful in understanding the LOS phenomena and providing a necessary condition for stability, they cannot alone be used for predicting the dynamical response of the frequency estimation of each converter. To capture this, the PLL dynamics need to be included to construct a large-signal reduced-order nonlinear model of the synchronization stability. This is done by taking the q-axes voltages in (7), (11), (15), used to derive the necessary stability conditions, and attaching the synchronizing PLL dynamics to this simplified q-axis voltage model. This
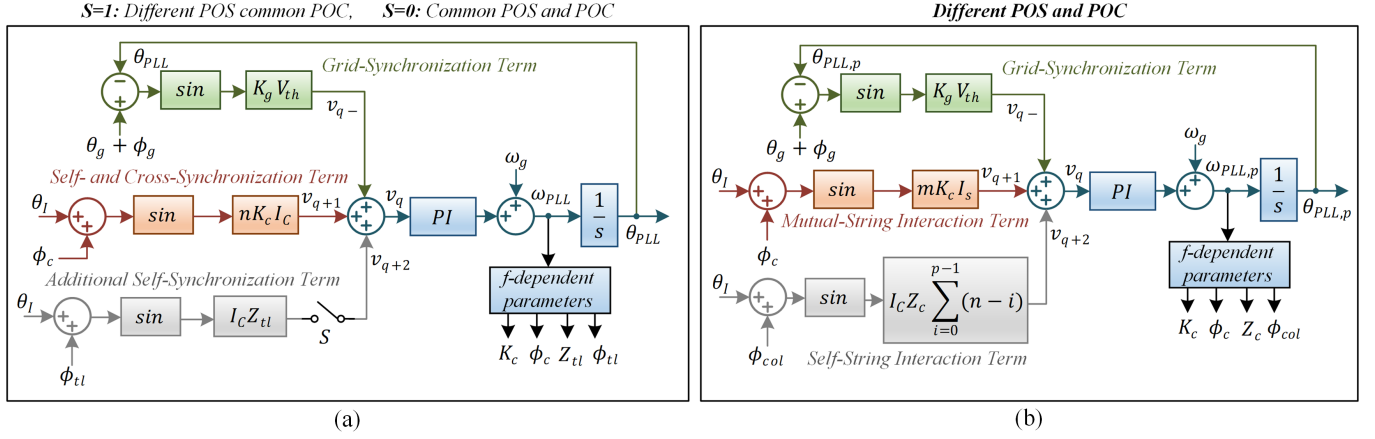
Fig. 4. Reduced-order quasi-static large-signal models for (a): parallel converters with common POS and POC (S open), from the configuration in Fig. 1, and paralleled converters with different POS but common POC (S closed), from the configuration in Fig. 2, and (b): parallel converters with different POS and POC, from the configuration in Fig. 3. For subfigure (b), this is shown for the pth PLL-synchronized converter in a wind farm string.

procedure describes the link between the formulation of the necessary stability conditions and the development of the reduced-order models.

The large-signal reduced-order nonlinear models of the three system configurations from Section II are shown in Fig. 4 where the simplified q-axes voltage equations derived are combined with the second-order PLL model. The block calculating the frequency-dependent parameters computes the actual impedance of a given line segment based on the static inductance of that segment and the operating frequency estimated by the PLL, e.g. $X = L\omega_{PLL}$. For the first two system configurations contained in Fig. 4(a), the estimated converter frequency is either identical or nearly identical for the n paralleled converters due to the shared POC. Therefore, only one frequency estimation needs to be modeled as shown in Fig. 4(a). However, for the system topology where paralleled converters are interconnected as for a wind farm string, there exists a significant impedance between the converters, which implies that the estimated PLL frequency of the paralleled converters will be different during transient conditions. This effect is captured using the large-signal reduced-order model in Fig. 4(b), where the PLL frequency estimated by the pth converter is modeled. It should be noted with this reduced-order model that the n models for the n paralleled converters are not coupled. This means that for a given fault condition, some converters may be unstable, whereas others will remain stable depending on the location in the wind farm string. Such a modeling approach does not represent a real scenario where the estimated frequencies are coupled as modeled for two paralleled converters in [28]. For power networks involving potential low-inertia systems, the frequency cannot be viewed as a global parameter in the initial contingency phase [51]. Therefore, as comprehensively studied in [51], different units may oscillate at different angular frequencies during a fault depending on their coupling to each other. However, since the collector grid impedances are much smaller than the park transformer and the transport cables, the difference in admittance distance (which can be used for coherency identi-
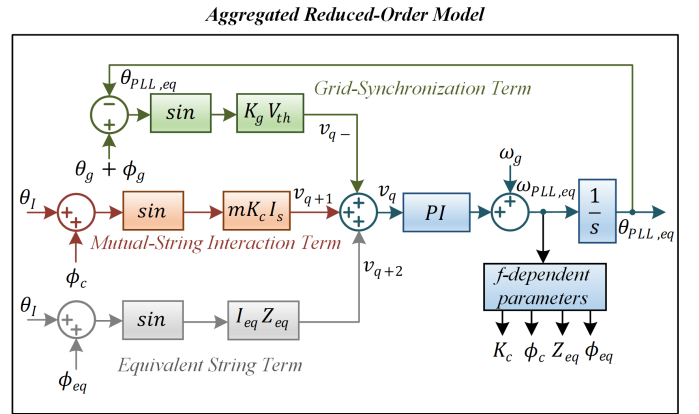

Fig. 5. Aggregated reduced-order quasi-static large-signal model for parallel converters with different POS and POC where all converters are represented as an equivalent frequency estimation.

fication [52]) from each converter to the fault location is small. Hence, the internal converters tend to synchronize coherently since they are strongly coupled to one another [53]–[55]. Due to this synchronization consensus, which implies that either all converters will experience synchronization instability or neither will, such converters can be grouped and their transient stability can be analyzed as a whole [56], [57]. Thus, despite the already simplified structure of the model, the intrinsic coherency feature of the string converters can be used to aggregate and reduce the model even further. This is useful when performing many consecutive cases to identify stability boundaries and parameter trends.

A. Aggregated Model for Wind Farm String

To be able to capture the frequency consensus among the n paralleled converters for the system topology where the converters have a different POS and POC, without having to model the frequency-couplings between all interconnected converters, an aggregated model is here proposed to assess the large-signal synchronization stability.

The reduced-order aggregated model in Fig. 5 uses an equivalent impedance of the wind farm string/collector system to preserve the collective dynamics of the internal frequency by coupling the PLL dynamics with the equivalent impedance. This aggregated reduced-order model only contains one frequency component, as visualized in Fig. 5 where Z_{eq}, ϕ_{eq}, and I_{eq} represent the magnitude and phase angle of the equivalent impedance and the total injected current of the entire string. To that end, the model aggregation is developed around the reduced-order quasi-static large-signal models from Fig. 4. Two different aggregation methods are examined, and a combination of them is employed in this work. These include a method preserving the total apparent power loss of the wind farm string ($Z_{eq,S}$) [32], [58], [59], and a method preserving the average voltage drop along the string ($Z_{eq,\Delta V}$) [60, p. 177].

1) Preservation of Apparent Power: The total power loss in the wind farm string is

$$S_{tot} = I_C^2 \sum_{i=1}^{n}(n-i+1)^2 Z_{c,i} + I_C^2 n Z_{tl} = I_{eq}^2 Z_{eq,S}. \quad (26)$$

Since $I_{eq} = nI_C$ is the total current of the collector system, the equivalent impedance can be found as

$$Z_{eq,S} = \frac{1}{n}Z_{tl} + \frac{1}{n^2}\sum_{i=1}^{n}(n-i+1)^2 Z_{c,i}. \quad (27)$$

2) Preservation of Average Voltage Drop: For this method, the averaged voltage drop on the impedances in the wind farm string can be expressed as

$$\Delta V_{avg} = \frac{1}{n}\left(\sum_{i=1}^{n} I_C(n-i+1)Z_{c,i} + I_C n Z_{tl}\right) = I_{eq}Z_{eq,\Delta V}. \quad (28)$$

Again by assuming equal current injections from all converters, the equivalent impedance can be isolated as

$$Z_{eq,\Delta V} = \frac{1}{n}Z_{tl} + \frac{1}{n}\sum_{i=1}^{n}(n-i+1)Z_{c,i}, \quad (29)$$

3) Weighted-Sum Equivalencing: Since the loss of synchronization fundamentally is a power transfer issue, the total apparent power of the entire wind farm string and the equivalent representation should be preserved. However, as described in [32], [61], this method may not be accurate, and it is observed from simulation studies in this work that the method may underestimate the impedance whereas the method on averaged voltage drop is observed to overestimate the equivalent impedance. Therefore, to avoid using a more complicated modeling framework with shunt impedances considered, a weighted sum of the two presented equivalencing methods is performed to get a better estimate of the equivalent impedance. This is

$$Z_{eq} = kZ_{eq,S} + (1-k)Z_{eq,\Delta V} \quad k \in [0, 1]. \quad (30)$$

Based on numerous simulations of the under/over-estimation using either method, it is found that $k = 0.75$ is a good compromise between the two. The reason for performing a weighted sum of the methods is due to the overlook of the network capacitance in the equivalent impedance. The systems with a higher network capacitance possess a slightly better result with a higher value of k. Along these lines, a lower k is slightly better for networks with a low capacitive effect. This is because the power flow is highly dependent on the network capacitances, due to their provision of reactive power [62]. Attaining better results by fine-tuning k may be achieved using an optimization algorithm where the error between the initial frequency drop at the fault instant of the aggregated model and the center of frequency drop of the n converters is minimized. Alternatively, the equivalent impedance may take into account the network capacitance, resulting in a more complicated equivalent impedance representation and, hence, a higher-order aggregated model, or by adjusting the equivalent impedance to match the power flows before and after aggregation, as it is done in [32]. Neither of these methods will be analyzed in this work since a highly simplified structure is desired and, as will be shown later, the selection of k around the value 0.75 has a small influence on the stability prediction capability, which is the main focus here.

IV. Model Validation

The developed static and dynamic models are verified against a detailed full-order simulation study performed in MATLAB's Simulink with PLECS blockset. All paralleled converters under test are operated with the grid-following control structure shown in Fig. 6 with an averaged representation of the converter switching actions, meaning that the converter terminal reference voltage is directly applied to three dependent voltage sources in the simulation [63]. The full representation of the converter in Fig. 6 is in the following analysis referred to as the full-order converter model. During severe faults, where the instability phenomenon is characterized by the fundamental frequency component, there is no loss of accuracy when employing an average model [5]. The network and controller parameters are as listed in Table I. The PLL parameters are designed for a damping ratio of 0.707 and a bandwidth of 20 Hz. Instead of specifying values for Z_{th} and Z_{fe}, the grid fault is simulated using a voltage source with a controlled amplitude at the bus to the right of Z_L. This implies that $V_{th}K_g = V_F$.

The model validation for the system with a common POS and POC, and different POS but a common POC is shown in Fig. 7, representing the system cases from Section II-A and Section II-B, respectively. Based on the nominal current injection and network parameters from Table I, the critical fault voltage magnitude from (8) and (12) is $V_F = 0.123$ pu. Hence, if the fault voltage magnitude drops below this value, instability will occur according to the static stability condition. As seen in Fig. 7(a)-(b), the system clearly becomes unstable when the static stability limit is not fulfilled. To that end, the reduced-order large-signal model depicted by dashed red is capable of capturing the instability and dynamical response. Fig. 7(c)-(d) show the results for three paralleled converters with a different POS but common POC, the configuration in Fig. 2, Section II-B. Despite the static stability limit not
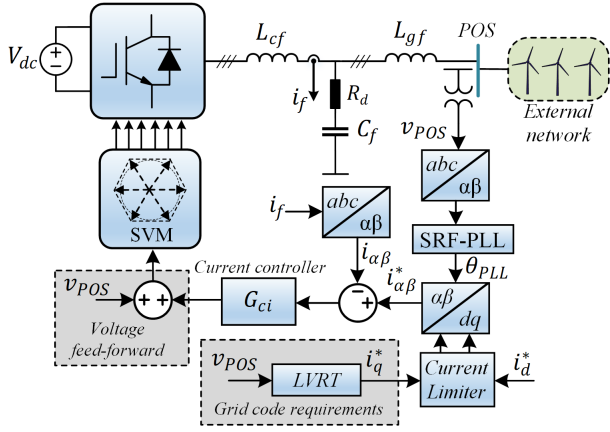
Fig. 6. Grid-following voltage-oriented control structure of each individual converter connected to the external network used for the full-order simulation model comparison.

TABLE I
CONTROL AND NETWORK PARAMETERS

| Symbol	Description	Value
V_b	Nominal grid voltage (line-line, rms)	400 V
I_C	Converter phase current magnitude	15 A
f_0	Rated frequency	50 Hz
L_{cf}	Converter-side inductor	0.07 pu
L_{gf}	Grid-side inductor	0.04 pu
C_f	Filter capacitor	0.07 pu
R_d	Filter damping resistance	0.02 pu
Z_L	Line impedance	$0.04 + 0.1j$ pu
Z_{tl}	Transformer leakage reactance	$0.05j$ pu
Z_c	Collector impedance	$0.0091 + 0.009j$ pu
K_{pc}	Current controller K_p	20 Ω
K_{rc}	Current controller K_r	2000 Ω/s
K_p^*	Initial PLL Design of K_p	0.3542 $[rad/(Vs)]$
K_i^*	Initial PLL Design of K_i	0.4509 $[rad/(Vs^2)]$
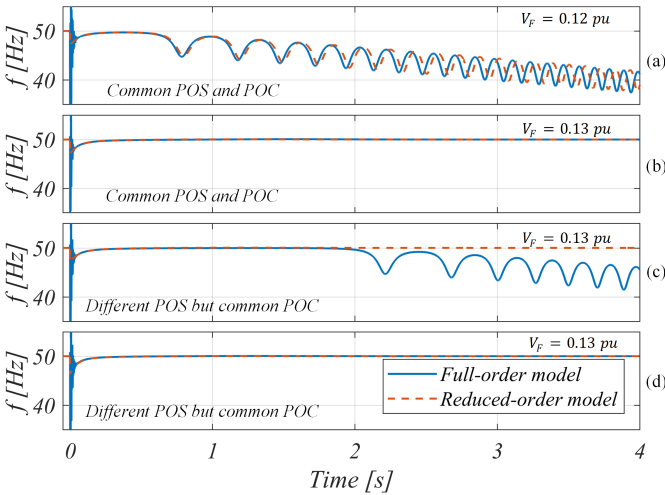
Fig. 7. Frequency responses of the full-order simulation model and reduced-order large-signal models for different cases and system configurations. The static stability limit or critical V_F is 0.123 pu for all cases. Three paralleled converters, as shown in Fig. 1 during a grid fault with $V_F = 0.13$ pu and $V_F = 0.12$ pu are shown in (a) and (b), respectively. (c): Three paralleled converters, as shown in Fig. 2 during a grid fault with $V_F = 0.13$ pu. (d): Same as (c) but with an increased damping ratio of the PLL dynamics ($K_p = 1.2K_p^*$).
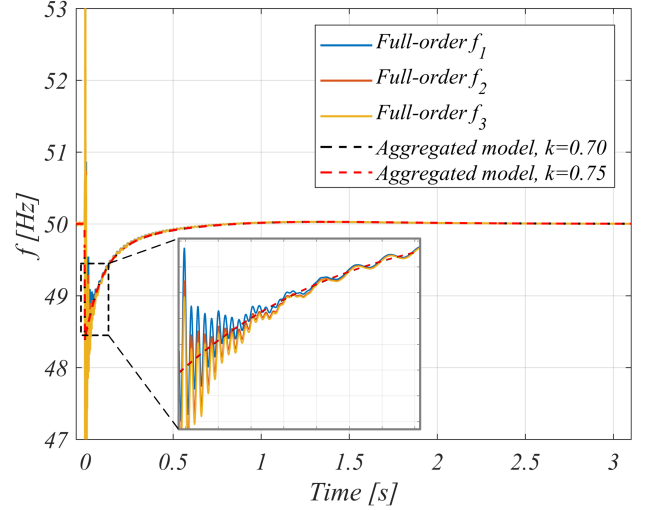

Fig. 8. Aggregated model accuracy shown with the frequency response of three paralleled full-order string converter models during a stable fault response with $V_F = 0.08$ pu. $f_1 - f_3$ denote the estimated frequency of each of the three paralleled full-order converter models where converter 3 is located at the far end of the string.

being different from the previous case, due to the assumption of perfect tracking in the inner current controller, the added transformer leakage inductance adds a destabilizing effect during the transient for the full-order representation. This destabilizing effect is not captured by the large-signal reduced-order model in Fig. 4(a) since it is assumed that θ_I can be controlled to $-\pi/2$, instantaneously, effectively canceling the influence of the leakage inductance. This is a fundamental limitation of the reduced-order model, which implies that some conservatism must be included when using the reduced-order dynamical model for systems with different POS but common POC. This limitation occurs in cases where the stable operating points of the converters are very close to violating the stability border in (12). Under such a scenario, the non-ideal dynamics of the inner current controller start to have a decisive effect on the transient stability outcome, which cannot be predicted using the reduced-order model. However, it should be mentioned, that when the converter operating point is not very close to the stability boundary, the bandwidth of the inner current controller does not have a significant effect on the stability assessment [64]. Since the static stability limit is not violated in Fig. 7(c), one is able to stabilize the system by increasing the damping ratio of the PLL dynamics [13], [19], as shown in Fig. 7(d).

For the verification of the configuration from Section II-C and the proposed aggregated model, three paralleled converters as shown in Fig. 3 are considered where the collector impedance Z_c is as listed in Table I, and the external line impedance is set to $Z_L = 0.008 + 0.066j$ Ω. Both impedances contain shunt capacitance to analyze the findings from Section II-D. For the simulated results in this section, these are 4.3 μF and 336 μF for the collector impedance and external line impedance, respectively. Based on the static stability limit in (18), the critical fault voltage magnitude considering that each converter injects 1 pu reactive current is $V_F = 0.078$ pu.
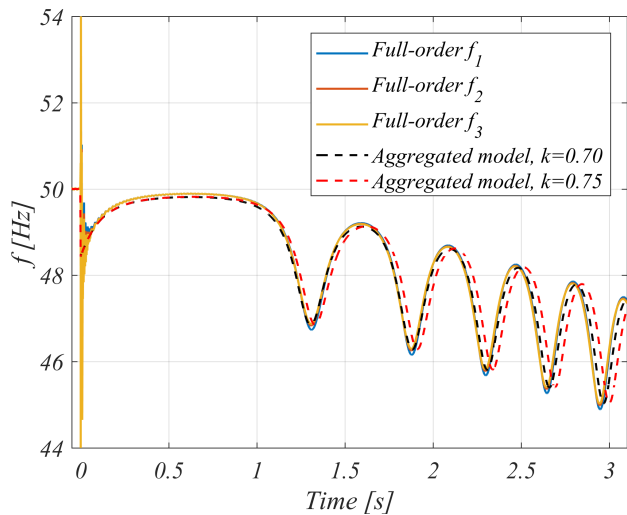
Fig. 9. Aggregated model accuracy shown with frequency responses of three paralleled full-order string converter models during an unstable fault response with $V_F = 0.07$ pu. $f_1 - f_3$ denote the estimated frequency of each of the three paralleled full-order converter models where converter 3 is located at the far end of the string.

Therefore, to verify this limit in addition to the reduced-order aggregated model, tests where $V_F = 0.07$ pu and $V_F = 0.08$ pu are conducted. The results for these two cases are shown in Fig. 8 and Fig. 9. At first, it is clear that the static stability limit can be accurately used as a necessary stability condition. This is true despite that the collector impedance and line impedance contains shunt capacitors, which verifies the assumption of neglecting the effect of shunt capacitances.

Furthermore, it is seen that the aggregated model for the collector system provides an accurate averaged behavior of the three paralleled converters with only a small deviation in the frequency response. For the aggregated model, the weighting factor k is slightly varied to show the impact on the response. For the stable case in Fig. 8, the difference is unnoticeable. For the unstable case in Fig. 9, it is seen that the accuracy of the modeled frequency can be improved by selecting $k = 0.7$ instead of $k = 0.75$. Even though the estimated frequency can be improved by selecting a different k, it is observed that the results obtained using $k = 0.75$ gives an excellent result in terms of stability assessment and transient response in the first and second swing of the response.

V. CASE STUDY ON ANHOLT WIND FARM

To get a realistic view of the static stability limitation from Section II-C and the proposed aggregated model, the detailed simulation model and these are compared considering the Anholt 400 MW offshore wind power plant (WPP) [66]. Anholt WPP is located approximately 20 km out of the eastern coast in Denmark and consists of 111 3.6 MW wind turbines [65]. The configuration of the wind turbines and the medium-voltage collector cable system can be seen in Fig. 10. Here it is evident that the assumption of a fixed collector impedance between all converters in a string is not realistic. This section aims to analyze a string of the Anholt WPP and the influence of different collector cable impedances on the synchronization

TABLE II
CABLE DATA USED FOR STUDYING THE ANHOLT WPP.

Cable Type	$R\,[m\Omega/km]$	$L\,[mH/km]$	$C\,[\mu F/km]$
Collector: $150\,mm^2$	124	0.39	0.19
Collector: $240\,mm^2$	75.4	0.36	0.23
Collector: $500\,mm^2$	36.6	0.32	0.32
Submarine cable	33.75	0.17	0.4
Land cable	33.75	0.56	0.17

stability under severe symmetrical grid faults. To that end, the accuracy of the proposed simplified aggregated model to evaluate the transient synchronization stability of a wind farm string is analyzed. The filter and control parameters used for the full-order model are as listed in Table I.

The distance between the turbines is approximately 600 meters at the edge and 900-1300 meters inside the farm [66]. These lengths, including the cable data from [50] (2XS(FL)2YRAA 18/30(36) kV), are used to calculate the impedance values for the cable Π-model of the collector system in Fig. 10. The data used for the export submarine and land cable can be found in [67], Table 49, and [68], Table 28, respectively. Both use aluminum $800\,mm^2$ conductors. A 25 km three-core submarine cable is used offshore, whereas three 59.6 km single-core cables laid in flat formation are used on land [49]. The impedance values for the cables are summarized in Table II. Both transformers are modeled as a pure reactance with 0.05 pu, whereas all shunt reactors are considered to absorb 120 MVAr. All impedance values are scaled depending on how many wind turbines are considered in the simulation study. I.e., the impedance of the export system will be scaled much larger when studying only one string compared to if all strings are operated at the same time. This is done to make sure that the voltage sensitivity at the PCC caused by each converter remains the same between different test cases.

A. Model Validation

For the wind farm string under study as highlighted in Fig. 10, the equivalent collector system impedance is calculated and used for the aggregated model. The critical fault voltage magnitude considering this system is $V_F = 0.0788$ pu. A stable and unstable response of the estimated frequencies of the wind farm string is shown in Fig. 11(a) and Fig. 11(b), respectively. A zoomed view of the initial transient behavior is shown from where all the estimated frequency of all nine string converters can be seen, and it is observed that the aggregated model accurately represents the averaged frequency component of the wind farm string.

As previously described, the time-domain transient response of the aggregated model can be improved by fine-tuning the weighting factor k. However, the initial value of $k = 0.75$ again provides an accurate response capable of assessing the transient stability as desired. Since the results in Fig. 11 contains a higher number of string converters and, hence, a higher network capacitance, than for the case presented in Fig. 8 and Fig. 9, a slightly higher value of k provides a better result due to the increased network capacitance.
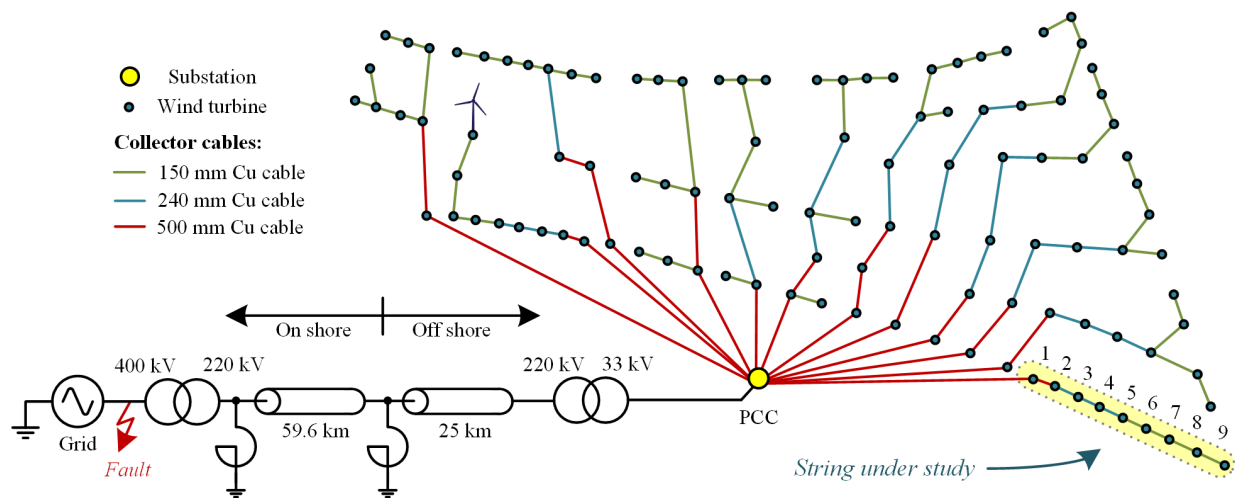
Fig. 10. The physical layout of Anholt 400 MW offshore wind power plant with the electrical export system and connections [49], [65]. One wind farm string with 9 wind turbines is under study for this work, as highlighted, where the string converter numbers are denoted.

With this, it is seen that the static stability limit, despite its simplicity, is highly accurate in determining the necessary condition for transient stability. To that end, this means that a system planner or designer can quickly assess whether a given system operation during a severe fault will be physically possible or not, without having to run a single simulation of the high-order system. In addition to the frequency plots in Fig. 12, the voltages and currents at the PCC and all converter connections points are shown for the same stable and unstable case in Fig. 12. The low-frequency instability oscillations are propagating the network voltage and currents. However, since all converters have tightly regulated currents, only a small impact is observed here. It should be noted that in Fig. 12, the currents deviate a bit from the 1 pu reference amplitude. This is because the currents displayed are the injected currents after the LC-filter and not the controlled converter-side current. Hence, the discrepancies between 1 pu and the injected currents originates from the discharge and charging of the filter capacitors during the fault.

B. Computational Enhancement

Using the proposed aggregated model, the 9 full-order paralleled wind turbine converters in the studied string including 11 3$^{\text{rd}}$-order cable models, transformers, and shunt reactors can accurately be represented as one single 2$^{\text{nd}}$-order nonlinear equation where the equivalent impedance and external line impedance are updated based on the estimated frequency.

A comparison of computational requirements for the proposed aggregated model and the full-order model is performed by measuring the time needed to solve one second of the fault response when a fault occurs. The computations are performed on a Lenovo ThinkPad with 8 GB of RAM, a 2.80 GHz Intel Core i7-7600U processor, and a Windows 10 64-bit operating system. The models are implemented in MATLABs Simulink version 2017a using PLECS blockset version 4.1.1. The simulation model is solved using the variable step size auto-solver in Simulink with a maximum step size and a relative tolerance of 1e-4 and 1e-3, respectively. The time

TABLE III
COMPARISON OF COMPUTATIONAL TIME FOR SOLVING 1 S OF ANHOLT
WIND FARM STRING USING DIFFERENT MODELS.

Switching Model	Average Model (full-order)	Aggregated Model
642 s	34.8 s	306 ms

needed to compute one-second fault response of the Anholt WPP string using a full-order switching model, a full-order average model, and the proposed simplified model is shown in Table III. The result for the switching model is estimated based on the time needed to compute a 40 ms response, whereas the time shown for the averaged and simplified models is an average of 100 different simulation runs. As evident, besides correctly predicting the stability outcome, the computational requirements can be significantly reduced. It is approximately 100 times faster than the averaged model and more than 2,000 times faster than the full-order switching model. For the comparison performed here, the switching frequency was set to 2 kHz. Accordingly, when the number of desired case studies increases, such as for identifying stability boundaries and parameter trends, and when the number of paralleled and interconnected converters increases, the benefit of using the simplified reduced-order aggregated model rapidly increases.

C. Evaluation of Assumptions

The presented reduced-order aggregated model is based on several assumptions including homogeneous VSC controller parameters and loading levels. Since these may affect the effectiveness and applicability of the model, these assumptions are evaluated in the following.

1) Heterogeneous Loading Levels and Current Controller Dynamics: First, the 9 converters in the string under study are exposed to different loading levels. The loading levels of the converters are linearly distributed between 0.6-1 pu to take into account wake effects [69]. To that end, the bandwidth of the inner current controller for each converter is different.
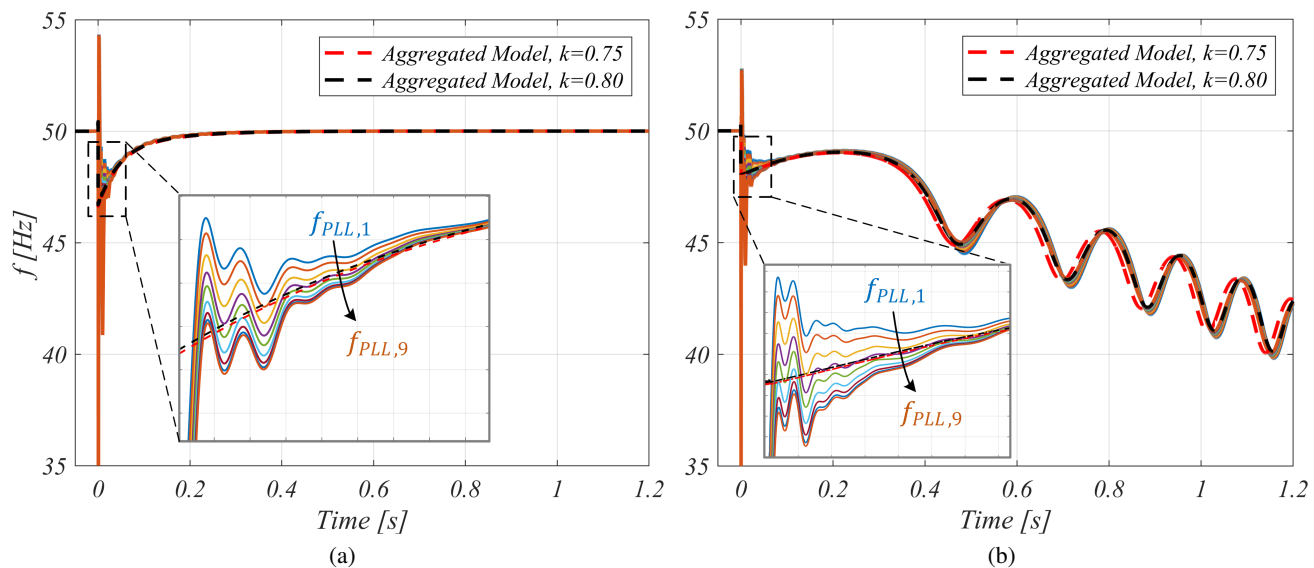
Fig. 11. Estimated PLL frequencies during a severe fault condition for full-order models and the proposed aggregated model. (a): Stable operating point with $V_F = 0.08$ pu. (b): Unstable operating point with $V_F = 0.07$ pu.

(a) Stable operating point with $V_F = 0.08$ pu.   (b) Unstable operating point with $V_F = 0.07$ pu.
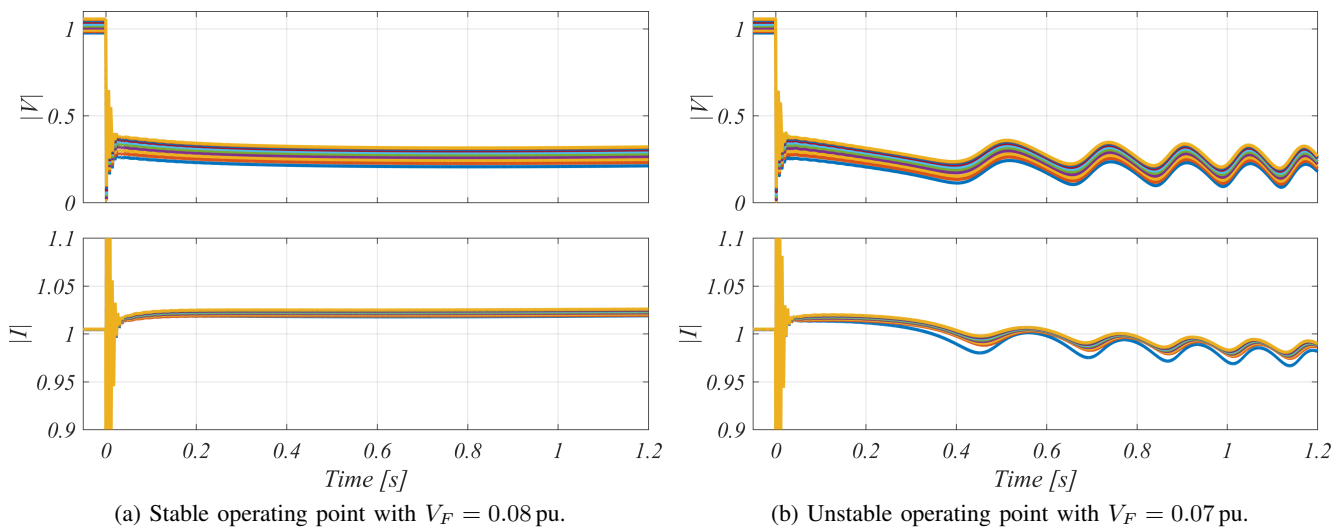
Fig. 12. The signal amplitudes of all nine POS voltages and the PCC voltage are displayed in the top figures. The amplitudes of all injected converter currents and the current at the PCC are shown in the bottom figures. All variables are shown in per-unit values during a severe grid fault.

Here, the bandwidths of the current controllers are linearly distributed between a $+20\%$ and a -20% in bandwidth compared to the initial design. This heterogeneous system is then compared with the proposed aggregated model under two severe fault conditions. One, where a stable operating point exists during the fault, and one where the operating point is unstable. The results of this are shown in Fig. 13. Despite the different loading levels of the converter before the fault and different dynamics of the inner current controllers, the aggregated reduced-order model is well capable of reproducing the synchronization behavior of the string.

2) Impact of PLL Bandwidth: Since the assumption of neglecting the inner current dynamics in the aggregated model is justifiable when the PLL dynamics are tuned slow, the performance of the aggregated model is here analyzed when the PLL bandwidth is increased. At the same time, the different loading levels of the converters are considered. The results for

this is shown in Fig. 14 for a PLL bandwidth of 60 Hz and a PLL bandwidth of 100 Hz. Despite, some discrepancies in the frequency estimation overshoot for the 100 Hz PLL case, the aggregated model still persists a good reproduction of the synchronization dynamics of the system.

3) Impact of Outer Loop Control: As mentioned in Section II, it is assumed that the outer control loops of the converter can be neglected during the fault. This is the case since the converter current references are switched to comply with the LVRT requirements during a severe fault. Accordingly, the outer direct voltage control (DVC) and alternating voltage control (AVC), controlling d-axis and q-axis current references through the dc-link voltage regulation and AC voltage magnitude, respectively, have a small impact on the synchronization stability during the fault. This assumption is justified in the following. The outer loops of a grid-side wind turbine converter do usually comprise a DVC for the d-axis
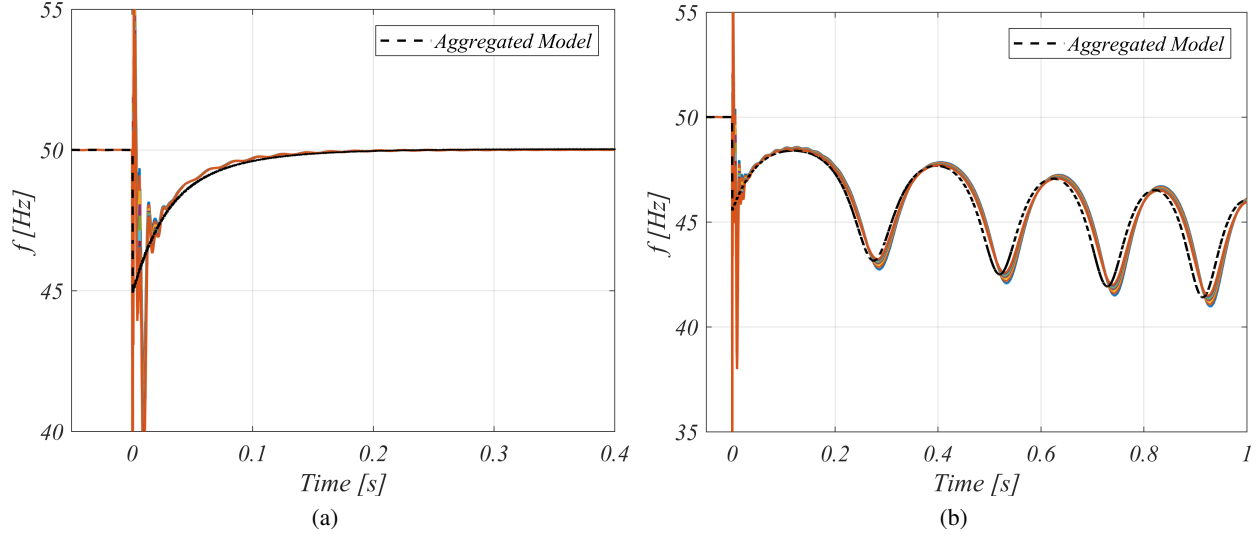
Fig. 13. Estimated PLL frequencies during a severe fault condition for full-order models and the proposed aggregated model for different converter parameters. All string converters operate at different loading levels from $0.6 - 1$ pu and different current controller bandwidths in the range $+20\%$ to -20%. $k = 0.75$. (a): Stable operating point with $V_F = 0.1$ pu. (b): Unstable operating point with $V_F = 0.05$ pu.
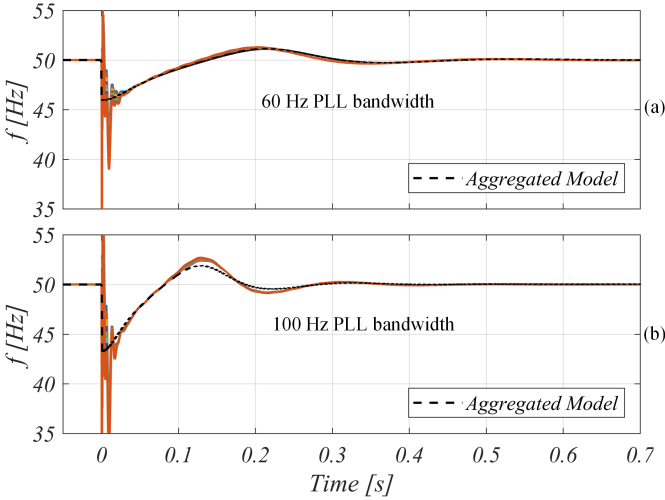

Fig. 14. Frequency responses of the full-order simulation model and aggregated model for different PLL bandwidths during a fault where $V_F = 0.1$ pu. $k = 0.75$. (a): PLL bandwidth of 60 Hz. (b): PLL bandwidth of 100 Hz.

Fig. 15. Current reference generation during normal operating conditions and during fault conditions. The DVC control i_d^* and the AVC control i_q^*. During fault conditions, reactive current support is prioritized from the LVRT requirements and the dc-link chopper control is activated to protect the dc-side from overvoltages. I_{WT} represents the current generated from the wind turbine generator-side converter.

control and an AVC for the q-axis control [70]. When a fault occurs, the current references are switched to comply with the grid code requirements, and a dc-side breaking chopper with PI control is used to stabilize the dc-link voltage during the fault and deal with the continuing turbine feed-in power. The chopper resistor R_{ch} is sized based on the input nominal power [70]. A detailed view of the outer loop control and the current reference generation during normal and faulted conditions are shown in Fig. 15. The outer DVC and AVC are tuned as in [71] with a bandwidth of 30 Hz and 10 Hz, respectively. The aggregated model is compared with the full-order string converters with outer loop control as shown in Fig. 15. This is conducted for two different fault conditions as shown in Fig. 16. As can be noticed, the dc-link voltages of the converters rapidly increase when the fault occurs due to the imbalance between dc-side and ac-side active power. However,

with the activation of the dc-side chopper control, the dc-link voltage is restored to its nominal voltage. Also, as can be seen in Fig. 16(b), the ac-side low-frequency oscillations are present in the dc-link voltages as well. Additionally, the q-axis current component has a non-zero value prior to the fault due to the inclusion of the AVC. Yet, with the outer loops considered, the aggregated model well reproduces the synchronization dynamics of the faulted system. This is the

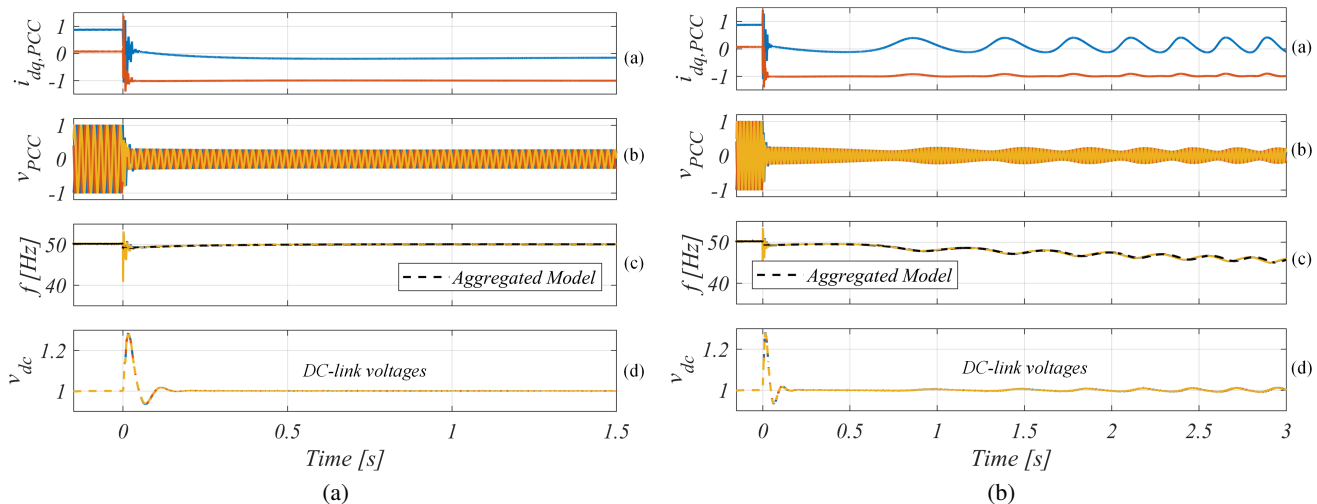Fig. 16. Comparison of aggregated model to full-order model with outer control loops (DVC: Direct Voltage Control and AVC: Alternating Voltage Control) during severe faults. The subfigures contain (a): dq-referenced PCC current, (b): three-phase PCC voltages, (c): Full-order converter PLL frequencies and estimated frequency of aggregated model, and (d): dc-link voltages of full-order converters with outer loop control. For the aggregated model $k = 0.75$. Left-side figure (a): Stable operating point with $V_F = 0.1$ pu. Right-side figure (b): Unstable operating point with $V_F = 0.05$ pu.

case for when a stable operation point exists, as shown in Fig. 16(a), and when the operating point during the fault is unstable, see Fig. 16(b).

VI. CONCLUSION

In this article, the modeling, analysis, and transient stability assessment of different paralleled multi-converter systems are addressed. From a modeling framework based on static conditions, the necessary conditions for transient stability are derived. The q-axes voltage components adopted to derive the necessary conditions are together with the dynamics of the synchronization unit used to develop reduced-order models for different multi-converter systems. Considering a daisy-chain collector system configuration where a non-negligible impedance separates each paralleled converter, an aggregated reduced-order model is proposed to represent the averaged frequency response of all paralleled converters. Both the static stability conditions and the aggregated models are verified through numerous simulation studies verifying their high accuracy for large-signal synchronization stability assessment. Then, the Anholt wind power plant is considered as a case study where the aggregated model is compared to the detailed operation of a wind farm string. High model accuracy is observed using the aggregated model, and the computational burden required for solving the system is reduced with a factor of 100 compared to the full-order system, which enables analysis of larger-scale systems. Finally, the assumptions used to derive the aggregated model is evaluated where a comparison has been made to a heterogeneous converter system operated at different loading levels with different current controller dynamics. Here, the impact of the PLL bandwidth and the introduction of outer control loops have also been analyzed, showing, still, great applicability of the proposed aggregated model to reproduce the synchronization dynamics of the system. Therefore, with low computational requirements and high accuracy, the presented analysis and proposed modeling

can effectively be applied as a screening tool and a convenient approach for early-stage fault analysis of a system design.

REFERENCES

[1] B. Kroposki, B. Johnson, Y. Zhang, V. Gevorgian, P. Denholm, B. M. Hodge, and B. Hannegan, "Achieving a 100 % renewable grid: Operating electric power systems with extremely high levels of variable renewable energy," *IEEE Power Energy Mag.*, vol. 15, no. 2, pp. 61–73, March 2017.

[2] VDE, "VDE-AR-N 4110: Technical requirements for the connection and operation of customer installations to the medium-voltage network (TCC medium-voltage)," 2017.

[3] Ö. Göksu, R. Teodorescu, C. L. Bak, F. Iov, and P. C. Kjær, "Instability of wind turbine converters during current injection to low voltage grid faults and PLL frequency based stability solution," *IEEE Trans. Power Syst.*, vol. 29, no. 4, pp. 1683–1691, July 2014.

[4] NationalGrid, UK, "Performance of phase-locked loop based converters," Tech. Rep., 2017.

[5] M. G. Taul, X. Wang, P. Davari, and F. Blaabjerg, "An overview of assessment methods for synchronization stability of grid-connected converters under severe symmetrical grid faults," *IEEE Trans. Power Electron.*, vol. 34, no. 10, pp. 9655–9670, Oct 2019.

[6] I. Erlich, F. Shewarega, S. Engelhardt, J. Kretschmann, J. Fortmann, and F. Koch, "Effect of wind turbine output current during faults on grid voltage and the transient stability of wind parks," in *Proc. IEEE PESGM*, July 2009, pp. 1–8.

[7] D. Dong, B. Wen, D. Boroyevich, P. Mattavelli, and Y. Xue, "Analysis of phase-locked loop low-frequency stability in three-phase grid-connected power converters considering impedance interactions," *IEEE Trans. Ind. Electron.*, vol. 62, no. 1, pp. 310–321, Jan 2015.

[8] X. He, H. Geng, and G. Yang, "Synchronization stability analysis of grid-tied power converters under severe grid voltage sags," in *Proc. IEEE PEAC*, Nov 2018, pp. 1–6.

[9] Q. Hu, L. Fu, F. Ma, and F. Ji, "Large signal synchronizing instability of PLL-based VSC connected to weak AC grid," *IEEE Trans. Power Syst.*, vol. 34, no. 4, pp. 3220–3229, July 2019.

[10] W. Wang, G. M. Huang, P. Kansal, L. E. Anderson, R. J. O'Keefe, D. Ramasubramanian, P. Mitra, and E. Farantatos, "Instability of PLL-synchronized converter-based generators in low short-circuit systems and the limitations of positive sequence modeling," in *Proc. IEEE NAPS*, Sep. 2018, pp. 1–6.

[11] M. G. Taul, X. Wang, P. Davari, and F. Blaabjerg, "Grid synchronization of wind turbines during severe symmetrical faults with phase jumps," in *Proc. IEEE ECCE*, Sept 2018, pp. 38–45.

[12] Q. Hu, J. Hu, H. Yuan, H. Tang, and Y. Li, "Synchronizing stability of DFIG-based wind turbines attached to weak AC grid," in *Proc. IEEE ICEMS*, Oct 2014, pp. 2618–2624.

[13] H. Wu and X. Wang, "Design-oriented transient stability analysis of pll-synchronized voltage-source converters," *IEEE Trans. Power Electron.*, vol. 35, no. 4, pp. 3573–3589, April 2020.

[14] H. Geng, L. Liu, and R. Li, "Synchronization and reactive current support of PMSG-based wind farm during severe grid fault," *IEEE Trans. Sust. Energy*, vol. 9, no. 4, pp. 1596–1604, Oct 2018.

[15] S. Ma, H. Geng, L. Liu, G. Yang, and B. C. Pal, "Grid-synchronization stability improvement of large scale wind farm during severe grid fault," *IEEE Trans. Power Syst.*, vol. 33, no. 1, pp. 216–226, Jan 2018.

[16] X. He, H. Geng, R. Li, and B. C. Pal, "Transient stability analysis and enhancement of renewable energy conversion system during LVRT," *IEEE Trans. Sust. Energy*, pp. 1–1, 2019.

[17] H. Wu and X. Wang, "An adaptive phase-locked loop for the transient stability enhancement of grid-connected voltage source converters," in *Proc. IEEE ECCE*, Sep. 2018, pp. 5892–5898.

[18] M. G. Taul, X. Wang, P. Davari, and F. Blaabjerg, "Robust fault ride through of converter-based generation during severe faults with phase jumps," *IEEE Trans. Ind. Appl.*, vol. 56, no. 1, pp. 570–583, Jan 2020.

[19] ——, "Systematic approach for transient stability evaluation of grid-tied converters during power system faults," in *Proc. IEEE ECCE*, Sep. 2019, pp. 5191–5198.

[20] H. Wu and X. Wang, "Transient stability impact of the phase-locked loop on grid-connected voltage source converters," in *IEEE Proc. ECCE Asia*, May 2018, pp. 2673–2680.

[21] H. Wu and X. Wang, "Design-oriented transient stability analysis of grid-connected converters with power synchronization control," *IEEE Trans. Ind. Electron.*, vol. 66, no. 8, pp. 6473–6482, Aug 2019.

[22] M. G. Taul, X. Wang, P. Davari, and F. Blaabjerg, "An efficient reduced-order model for studying synchronization stability of grid-following converters during grid faults," in *2019 20th Workshop on Control and Modeling for Power Electronics (COMPEL)*, June 2019, pp. 1–7.

[23] S. Shah and P. Sensarma, "Auto-synchronization of lc filter based front-end converter with parallel inverters based weak distorted island grid using voltage injection," in *IECON 2012 - 38th Annual Conference on IEEE Industrial Electronics Society*, Oct 2012, pp. 3388–3393.

[24] L. Huan, H. Xin, W. Dong, and F. Dörfler, "Impacts of grid structure on pll-synchronization stability of converter-integrated power systems," *arXiv:1903.05489v2*, Nov 2019.

[25] B. Wen, D. Dong, D. Boroyevich, R. Burgos, P. Mattavelli, and Z. Shen, "Impedance-based analysis of grid-synchronization stability for three-phase paralleled converters," *IEEE Trans. Power Electron.*, vol. 31, no. 1, pp. 26–38, Jan 2016.

[26] R. Rosso, M. Andresen, S. Engelken, and M. Liserre, "Analysis of the interaction among power converters through their synchronization mechanism," *IEEE Trans. Power Electron.*, vol. 34, no. 12, pp. 12 321–12 332, Dec 2019.

[27] D. Dong, B. Wen, P. Mattavelli, D. Boroyevich, and Y. Xue, "Grid-synchronization modeling and its stability analysis for multi-paralleled three-phase inverter systems," in *IEEE Proc. APEC*, March 2013, pp. 439–446.

[28] J. Zhao, M. Huang, and X. Zha, "Transient stability analysis of grid-connected vsis via pll interaction," in *2018 IEEE International Power Electronics and Application Conference and Exposition (PEAC)*, Nov 2018, pp. 1–6.

[29] A. M. S. Al-bayati, F. Mancilla-David, and J. L. Domínguez-Garcíal, "Aggregated models of wind farms: Current methods and future trends," in *2016 North American Power Symposium (NAPS)*, 2016, pp. 1–6.

[30] W. Li, A. M. Gole, M. K. Das, and I. Kaffashan, "Research on wind farms aggregation method for electromagnetic simulation based on fdne," in *2019 IEEE PES Innovative Smart Grid Technologies Europe (ISGT-Europe)*, 2019, pp. 1–5.

[31] M. Altin, . Göksu, A. D. Hansen, and P. E. Sørensen, "Aggregated wind power plant models consisting of iec wind turbine models," in *2015 IEEE Eindhoven PowerTech*, 2015, pp. 1–5.

[32] J. Martínez-Turégano, S. Añó-Villalba, G. Chaques-Herraiz, S. Bernal-Perez, and R. Blasco-Gimenez, "Model aggregation of large wind farms for dynamic studies," in *IECON 2017 - 43rd Annual Conference of the IEEE Industrial Electronics Society*, Oct 2017, pp. 316–321.

[33] A. P. Gupta, A. Mohapatra, and S. N. Singh, "Apparent power loss based equivalent model of wind farm collector system," in *2018 20th National Power Systems Conference (NPSC)*, 2018, pp. 1–6.

[34] W. Du, W. Dong, H. Wang, and J. Cao, "Dynamic aggregation of same wind turbine generators in parallel connection for studying oscillation stability of a wind farm," *IEEE Trans. Power Syst.*, vol. 34, no. 6, pp. 4694–4705, 2019.

[35] P. Wang, Z. Zhang, Q. Huang, N. Wang, X. Zhang, and W. Lee, "Improved wind farm aggregated modeling method for large-scale power

system stability studies," *IEEE Trans. Power Syst.*, vol. 33, no. 6, pp. 6332–6342, 2018.

[36] R. Fang, R. Shang, M. Wu, C. Peng, and X. Guo, "Application of gray relational analysis to k-means clustering for dynamic equivalent modeling of wind farm," *International Journal of Hydrogen Energy*, vol. 42, no. 31, pp. 20 154–20 163, 2017.

[37] W. Teng, X. Wang, Y. Meng, and W. Shi, "An improved support vector clustering approach to dynamic aggregation of large wind farms," *CSEE Journal of Power and Energy Systems*, vol. 5, no. 2, pp. 215–223, 2019.

[38] W. Li, P. Chao, X. Liang, J. Ma, D. Xu, and X. Jin, "A practical equivalent method for dfig wind farms," *IEEE Trans. Sust. Energy*, vol. 9, no. 2, pp. 610–620, 2018.

[39] X. Zha, S. Liao, M. Huang, Z. Yang, and J. Sun, "Dynamic aggregation modeling of grid-connected inverters using hamilton's-action-based coherent equivalence," *IEEE Trans. Ind. Electron.*, vol. 66, no. 8, pp. 6437–6448, 2019.

[40] H. R. Ali, L. P. Kunjumuhammed, B. C. Pal, A. G. Adamczyk, and K. Vershinin, "Model order reduction of wind farms: Linear approach," *IEEE Trans. Sust. Energy*, vol. 10, no. 3, pp. 1194–1205, 2019.

[41] S. Vijayshankar, V. Purba, P. J. Seiler, and S. V. Dhople, "Reduced-order aggregate dynamical model for wind farms," in *2019 American Control Conference (ACC)*, 2019, pp. 5464–5471.

[42] J. Dai, Y. Tang, and Y. Wang, "Aggregation frequency response modeling for wind farms with frequency support capabilities," in *2019 IEEE Power Energy Society General Meeting (PESGM)*, 2019, pp. 1–5.

[43] J. Bi, W. Du, and H. F. Wang, "An aggregation method of wind farms model for studying power system low frequency power oscillation," in *2017 2nd International Conference on Power and Renewable Energy (ICPRE)*, 2017, pp. 422–427.

[44] R. M. G. Castro and J. M. Ferreira de Jesus, "A wind park reduced-order model using singular perturbations theory," *IEEE Trans. Energy Conv.*, vol. 11, no. 4, pp. 735–741, 1996.

[45] Y. Gu, N. Bottrell, and T. C. Green, "Reduced-order models for representing converters in power system studies," *IEEE Trans. Power Electron.*, vol. 33, no. 4, pp. 3644–3654, April 2018.

[46] M. G. Taul, X. Wang, P. Davari, and F. Blaabjerg, "Current reference generation based on next generation grid code requirements of grid-tied converters during asymmetrical faults," *IEEE J. Emerg. Sel. Topics Power Electron.*, pp. 1–1, 2019.

[47] B. Xie, L. Zhou, C. Zheng, and Q. Zhang, "Stability and resonance analysis and improved design of n-paralleled grid-connected pv inverters coupled due to grid impedance," in *IEEE Proc. APEC*, March 2018, pp. 362–367.

[48] J. L. Agorreta, M. Borrega, J. López, and L. Marroyo, "Modeling and control of n-paralleled grid-connected inverters with lcl filter coupled due to grid impedance in pv plants," *IEEE Trans. Power Electron.*, vol. 26, no. 3, pp. 770–785, March 2011.

[49] C. F. Jensen, "Harmonic background amplification in long asymmetrical high voltage cable systems," *Electric Power Systems Research*, vol. 160, pp. 292 – 299, 2018.

[50] Nexans. (2008) Submarine power cables. [Online]. Available: https://www.nexans.de/Germany/2010/NEX_SubmPowCables_mai08_1.pdf

[51] F. Milano, F. Dörfler, G. Hug, D. J. Hill, and G. Verbič, "Foundations and challenges of low-inertia systems (invited paper)," in *2018 Power Systems Computation Conference (PSCC)*, 2018, pp. 1–25.

[52] S. T. Y. Lee and F. C. Schweppe, "Distance measures and coherency recognition for transient stability equivalents," *IEEE Trans. Power Apparatus and Systems*, vol. PAS-92, no. 5, pp. 1550–1557, 1973.

[53] Z. Shuai, Y. Peng, X. Liu, Z. Li, J. M. Guerrero, and Z. J. Shen, "Dynamic equivalent modeling for multi-microgrid based on structure preservation method," *IEEE Trans. Smart Grid*, vol. 10, no. 4, pp. 3929–3942, 2019.

[54] A. M. Khalil and R. Iravani, "Power system coherency identification under high depth of penetration of wind power," *IEEE Trans. Power Syst.*, vol. 33, no. 5, pp. 5401–5409, 2018.

[55] S. Sastry and P. Varaiya, "Coherency for interconnected power systems," *IEEE Trans. Automatic Control*, vol. 26, no. 1, pp. 218–226, 1981.

[56] M. L. Ourari, L. Dessaint, and V. Do, "Dynamic equivalent modeling of large power systems using structure preservation technique," *IEEE Trans. Power Syst.*, vol. 21, no. 3, pp. 1284–1295, 2006.

[57] S. Zhao, N. C. Nair, and N. Vong, "Coherency-based equivalencing method for large wind farms," in *2009 IEEE Power & Energy Society General Meeting*, 2009, pp. 1–8.

[58] X. Su, Y. Liu, H. Song, and D. Xu, "Comparison between the two equivalent methods of collector system for wind farms," in *2015 International Conference on Estimation, Detection and Information Fusion (ICEDIF)*, Jan 2015, pp. 354–358.

[59] E. Muljadi, C. P. Butterfield, A. Ellis, J. Mechenbier, J. Hochheimer, R. Young, N. Miller, R. Delmerico, R. Zavadil, and J. C. Smith, "Equivalencing the collector system of a large wind power plant," in *2006 IEEE Power Engineering Society General Meeting*, 2006, pp. 9 pp.–.

[60] L. H. Kocewiak, "Harmonics in large offshore wind farms," Ph.D. dissertation, Faculty of Engineering and Science at Aalborg University, 2012.

[61] A. P. Gupta, A. Mohapatra, and S. N. Singh, "Apparent power loss based equivalent model of wind farm collector system," in *2018 20th National Power Systems Conference (NPSC)*, Dec 2018, pp. 1–6.

[62] J. Ruan, Z. Lu, Y. Qiao, and Y. Min, "Analysis on applicability problems of the aggregation-based representation of wind farms considering dfigs' lvrt behaviors," *IEEE Trans. Power Syst.*, vol. 31, no. 6, pp. 4953–4965, 2016.

[63] S. Bacha, I. Munteanu, and A. I. Bratcu, *Power Electronic Converters Modeling and Control with Case Studies*, 1st ed. Springer, 2014, ISBN: 978-1-4471-5477-8.

[64] X. He, H. Geng, and S. Ma, "Transient stability analysis of grid-tied converters considering PLL's nonlinearity," *CPSS Transactions on Power Electronics and Applications*, vol. 4, no. 1, pp. 40–49, March 2019.

[65] L. H. Kocewiak, B. L. . Kramer, O. Holmstrøm, K. H. Jensen, and L. Shuai, "Resonance damping in array cable systems by wind turbine active filtering in large offshore wind power plants," *IET Renewable Power Generation*, vol. 11, no. 7, pp. 1069–1077, 2017.

[66] Ørsted, DK. (2019) Anholt offshore wind farm. [Online]. Available: http://dise.org.pl/dania2019/AnholtOffshoreWindFarm.pdf

[67] ABB, "Xlpe submarine cable systems attachment to xlpe land cable systems - user's guide," Tech. Rep.

[68] ——, "Xlpe land cable systems - user's guide," Tech. Rep.

[69] S. Kuenzel, L. P. Kunjumuhammed, B. C. Pal, and I. Erlich, "Impact of wakes on wind farm inertial response," *IEEE Trans. Sust. Energy*, vol. 5, no. 1, pp. 237–245, 2014.

[70] M. H. Qais, H. M. Hasanien, and S. Alghuwainem, "Low voltage ride-through capability enhancement of grid-connected permanent magnet synchronous generator driven directly by variable speed wind turbine: a review," *The Journal of Engineering*, vol. 2017, no. 13, pp. 1750–1754, 2017.

[71] L. Harnefors, M. Bongiorno, and S. Lundberg, "Input-admittance calculation and shaping for controlled voltage-source converters," *IEEE Trans. Ind. Electron.*, vol. 54, no. 6, pp. 3323–3334, Dec 2007.

Xiongfei Wang (S'10-M'13-SM'17) received the B.S. degree from Yanshan University, Qinhuangdao, China, in 2006, the M.S. degree from Harbin Institute of Technology, Harbin, China, in 2008, both in electrical engineering, and the Ph.D. degree in energy technology from Aalborg University, Aalborg, Denmark, in 2013. Since 2009, he has been with the Department of Energy Technology, Aalborg University, where he became an Assistant Professor in 2014, an Associate Professor in 2016, a Professor and Research Program Leader for Electronic Power Grid (eGrid) in 2018, and the Director of Aalborg University-Huawei Energy Innovation Center in 2020. He is also a Visiting Professor of power electronics systems with KTH Royal Institute of Technology, Stockholm, Sweden. His current research interests include modeling and control of grid-interactive power converters, stability and power quality of power-electronic-based power systems, active and passive filters. Dr. Wang was selected into Aalborg University Strategic Talent Management Program in 2016. He has received six Prize Paper Awards at the IEEE Transactions and conferences, the 2016 Outstanding Reviewer Award of IEEE TRANSACTIONS ON POWER ELECTRONICS, the 2018 IEEE PELS Richard M. Bass Outstanding Young Power Electronics Engineer Award, the 2019 IEEE PELS Sustainable Energy Systems Technical Achievement Award, the 2019 Highly Cited Researcher by Clarivate Analytics (former Thomson Reuters), and the 2020 IEEE PES Prize Paper Award. He serves as a Member at Large for Administrative Committee of IEEE Power Electronics Society in 2020-2022, and as an Associate Editor for the IEEE TRANSACTIONS ON POWER ELECTRONICS, the IEEE TRANSACTIONS ON INDUSTRY APPLICATIONS, and the IEEE JOURNAL OF EMERGING AND SELECTED TOPICS IN POWER ELECTRONICS.

Pooya Davari (S'11–M'13-SM'19) received the B.Sc. and M.Sc. degrees in electronic engineering in 2004 and 2008, respectively, and the Ph.D. degree in power electronics from QUT, Australia, in 2013. From 2005 to 2010, he was involved in several electronics and power electronics projects as a Development Engineer. From 2013 to 2014, he was with QUT, as a Lecturer. He joined Aalborg University, in 2014, as a Postdoc, where he is currently an Associate Professor. He has been focusing on EMI, power quality and harmonic mitigation analysis and control in power electronic systems. He has published more than 140 technical papers. Dr. Davari served as a Guest Associate Editor of IET journal of Power Electronics, IEEE Access Journal, Journal of Electronics and Journal of Applied Sciences. He is an Associate Editor of Journal of Power Electronics, Associate Editor of IET Electronics, Editorial board member of EPE journal and Journal of Applied Sciences. He is member of the International Scientific Committee (ISC) of EPE (ECCE Europe) and a member of Joint Working Group six and Working Group eight at the IEC standardization TC77A. Dr. Davari is the recipient of a research grant from the Danish Council of Independent Research (DFF-FTP) in 2016, and 2020 IEEE EMC Society Young Professional Award for his contribution to EMI and Harmonic Mitigation and Modeling in Power Electronic Applications.

Mads Graungaard Taul (S'17) received the B.Sc. and M.Sc. degrees in electrical energy engineering with a specialization in power electronics and drives in 2016 and 2019, respectively, and the Ph.D. degree in power electronic systems from Aalborg University, Denmark in 2020. In connection with his M.Sc. degree, he received the 1st prize master's thesis award for excellent and innovative project work by the Energy Sponsor Programme. Dr. Taul was a visiting researcher at the University of California, Berkeley, at the Department of Electrical Engineering and Computer Science from August 2019 to January 2020. Currently, he is a Post-doctoral researcher at the Department of Energy Technology at Aalborg University, Denmark. His main research interests include renewable energy sources and grid-connected converters with a particular focus on modeling, control, and stability analysis of power electronics-based power systems.

Frede Blaabjerg (S'86–M'88–SM'97–F'03) was with ABB-Scandia, Randers, Denmark, from 1987 to 1988. From 1988 to 1992, he got the PhD degree in Electrical Engineering at Aalborg University in 1995. He became an Assistant Professor in 1992, an Associate Professor in 1996, and a Full Professor of power electronics and drives in 1998. From 2017 he became a Villum Investigator. He is honoris causa at University Politehnica Timisoara (UPT), Romania and Tallinn Technical University (TTU) in Estonia. His current research interests include power electronics and its applications such as in wind turbines, PV systems, reliability, harmonics and adjustable speed drives. He has published more than 600 journal papers in the fields of power electronics and its applications. He is the co-author of four monographs and editor of ten books in power electronics and its applications. He has received 32 IEEE Prize Paper Awards, the IEEE PELS Distinguished Service Award in 2009, the EPE-PEMC Council Award in 2010, the IEEE William E. Newell Power Electronics Award 2014, the Villum Kann Rasmussen Research Award 2014, the Global Energy Prize in 2019 and the 2020 IEEE Edison Medal. He was the Editor-in-Chief of the IEEE TRANSACTIONS ON POWER ELECTRONICS from 2006 to 2012. He has been Distinguished Lecturer for the IEEE Power Electronics Society from 2005 to 2007 and for the IEEE Industry Applications Society from 2010 to 2011 as well as 2017 to 2018. In 2019-2020 he serves a President of IEEE Power Electronics Society. He is Vice-President of the Danish Academy of Technical Sciences too. He is nominated in 2014-2019 by Thomson Reuters to be between the most 250 cited researchers in Engineering in the world.